Desalination and Water Treatment
www.deswater.com

doi: 10.5004/dwt.2019.24665

171 (2019) 18–28
December

Mass transfer mechanism of reverse osmosis concentrate brines with vacuum membrane distillation in arid areas

Juan Liu[a,b,c], Juncang Tian[a,b,c,*]

[a]*Ningxia University of School of Civil and Hydropower Engineering, No. 489, Helanshan West Road, Xixia District, Yinchuan City, Ningxia, China, Tel. +8615909618819, emails: slxtjc@163.com (J.C. Tian), nxdxlj1980@163.com (J. Liu)*
[b]*Ningxia Research Center of Technology on Water-saving Irrigation and Water Resources Regulation, No. 489, Helanshan West Road, Xixia District, Yinchuan City, Ningxia, China*
[c]*Engineering Research Center for Efficient Utilization of Water Resources in Modern Agriculture in Arid Regions, No. 489, Helanshan West Road, Xixia District, Yinchuan City, Ningxia, China*

Received 6 February 2019; Accepted 29 June 2019

ABSTRACT

An osmotic vapor pressure model was established based on the change of vacuum pressure on the permeate side with vapor temperature, and it was validated by experimental studies. Furthermore, a modified mass transfer model in reverse osmosis concentrate brines treated by vacuum membrane distillation in arid areas was proposed and also validated through experimental data. Utilizing this model, membrane properties such as pore size, porosity, thickness and pore tortuosity were employed to investigate the mass transfer mechanisms by simulation analysis. Additionally, the mass transfer mechanisms in different operational conditions were analyzed through experiments. The modified model may provide a potential tool to guide the production and selection of membranes in the future.

Keywords: Arid area; Mass transfer mechanism; Reverse osmosis concentrate brines; Vacuum membrane distillation

1. Introduction

In arid areas where precipitation is low, evaporation is high and water resources are naturally scarce, underground water as the major water-supply source is mainly brackish water containing high salt. Also it cannot be substituted by freshwater resources in most regions. Among numerous brackish water desalination techniques, reverse osmosis is the most advanced, effective and energy-efficient membrane separation technique up till now. At the same time, treatment and discharge of reverse osmosis concentrate brines have attracted extensive attention. The most common treatment method of reverse osmosis concentrate brines is directly discharging, which may lead to increment of mineralization degree of the underground water. Owing to small influence of solution concentration on feed side, membrane distillation (MD), a new membrane process, is suitable for reverse osmosis concentrate brines treatment. It combines the traditional distilling process with the membrane separation technique and utilizes vapor pressure deficit (VPD) between both sides of the hydrophobic microporous membrane as mass transfer force [1].

Compared with conventional separation methods, the superiority of vacuum membrane distillation (VMD) is instantiated in low operating temperature and pressure, facilitating feed liquid vaporization at atmospheric pressure. And it is also featured by low conductive heat loss and mass transfer resistance. Therefore, it possesses higher membrane flux than other types of membrane distillation. Through comparative analysis on heat and mass transfer characteristics of direct contact membrane distillation (DCMD), air gap membrane distillation (AGMD), sweeping gas membrane distillation (SGMD) and VMD, El-Bourawi et al. [2] proposed that heat loss, temperature polarization and concentration polarization are three major causes of low membrane flux of

* Corresponding author.

DCMD, AGMD and SGMD. They also pointed out that the high vacuum degree on the permeate side of VMD membrane substantially reduced conductive heat losses of high salt hot diet, which further resulted in relatively low thermal loss. Hence, water vapor flux of VMD is higher than that of DCMD [3].

Modeling is an effective tool to understand MD heat and mass transfer, simulation and process optimization design. Mengual et al. [4] established a VMD heat and mass transfer model for capillary membrane in shell-and-tube membrane modules. And they deemed that mass transfer model was associated with Knudsen diffusion and membrane flux relevant to heat transfer coefficient between the liquid of feed solution and the membrane surface, which were both verified by experimental data. Furthermore, they raised that heat exchange on the surface of porous membrane was different from that of rigid and non-porous surface. Li and Sirkar [3] set up a VMD heat and mass transfer model in a rectangular cross-flow pattern. And they found variations in vacuum pressure of the permeate side can be ignored due to short length of membrane fiber. Hence, the pressure of vacuum pump can be used as the vacuum pressure on permeate side. Abdallah et al. [5] built up a VMD flux model that neglected the influence of vapor pressure generated by osmotic vapor. They only considered the vacuum pressure provided by vacuum pump on the permeate side. Lee and Kim [6] put forward a 1-D VMD model to predict performance of seawater desalination, and to solve energy and momentum balance equations as well as heat and mass transfer formulas. Kim et al. [7] utilized molecular dynamics and statistical mechanics to interpret water vapor diffusion transfer along long and straight pores. They concluded that driving force of water vapor flux is the gradient of incidence, expressed in $P/\sqrt{T}$. The number of vapor molecules in the intermediate cross section passing straight pores can be figured out to estimate the vapor flux, which is further validated by experimental data. Liu et al. [8] investigated mass transfer processes during VMD of hollow fiber related to homogeneous membrane and heterogeneous membrane models. They pointed out that the Knudsen diffusion regardless of Knudsen number and the combination of viscous flow conditions preferably coincided with the experiment when osmotic flux was calculated. Florez et al. [9] adopted multi-scale numerical model to study mass transfer through a microporous artificial membrane, and established a two-dimensional numerical model of the parallel flow micro-device on the liquid side and the permeate side. Taherinejad et al. [10] investigated the porous medium model of hollow fiber water filtration system, and proposed a new model of fluid flow in hollow fiber membrane filtration module. Martijn et al. [11] developed a heat and mass transfer model for steady-state, multistage and semi-intermittent membrane distillation. Ma et al. [12] numerically studied the VMD and solar panel collector (FPC) integrated coupling module, and proposed the heat and mass transfer coupling model of solar VMD.

In addition, computational fluid dynamics (CFD) simulation has been extensively used to study membrane distillation. Wang et al. [13] designed a hollow fiber membrane module using CFD, and studied the influence of baffle on the flow-field distribution of the membrane module. Abdolbaghi et al. [14] simulated the process of heat and mass transfer in the separation of ethylene glycol solution by VMD, and presented a comprehensive model to study the effects of different VMD parameters on flat membrane modules. Based on CFD, the model adopts finite element method as a tool and solves different partial differential equations. Ma et al. [15] proposed a CFD porous medium model, in which the interaction between membrane fibers at different distances and locations was simulated. A hollow fiber membrane filtration device based on nine membrane fibers was constructed. The filtration performance of membrane fibers at different locations was simulated by CFD. Yang et al. [16] employed CFD to investigate the water recovery performance of nanoceramic membranes with different application time, and analyzed the influence of membrane fouling on heat and mass transfer. Yazgan-Birgi et al. [17] used CFD model to study the performance of DCMD process for flat and hollow fibers. A three-dimensional CFD model was established and validated by experimental data.

Considering investigations mentioned above, 1-D or 2-D heat and mass transfer models are established in different experimental conditions and then validated. However, simulation analysis on the influence of membrane structure (e.g., membrane pore size, membrane porosity, membrane thickness and membrane pore tortuosity) during VMD on flux has been rarely carried out. In the experiment, as vapor temperature on the permeate side changes, vacuum pressure on this side will also change despite that the vacuum pressure of vacuum pump is a constant value. The vacuum pressure on the permeate side under this circumstance has not been analyzed before. Here, a model that considers relationship between osmotic vacuum pressure and vapor temperature is established and then validated. Meanwhile, the mass transfer model is also modified and validated. On the basis of this mass transfer model, different membrane materials described in the literature are selected to conduct simulation analysis on mass transfer mechanism of diverse membrane structures. Furthermore, such mass transfer mechanisms are analyzed through experiment subjected to different operational conditions.

2. Materials and methods

2.1. Test and materials

2.1.1. Sources and compositions of reverse osmosis concentrate brines

Xinrong Village in Helan County of Yinchuan City, Ningxia Province was selected as a typical area in Northwest China. In the test, reverse osmosis concentrate brines was obtained from a greenhouse brackish water reverse osmosis desalination system with a freshwater yield of 3 m^3/h. Ratio of contributing water of freshwater to concentrate was defined to be 3:1. In this case, concentrate yield per hour was 1 m^3/h. Compositions of concentrate have been presented in Table 1.

2.1.2. VMD modules

PTFE hollow fiber hydrophobic microporous membrane with an average inner diameter of 1.2 mm, an average outer diameter of 2.3 mm, wall thickness of 0.5 mm, an average

Table 1
A table of reverse osmosis concentrate brines compositions

Ion species	Ca^{2+}	Mg^{2+}	K^{+}	Na^{+}	Cl^{-}	SO_4^{2-}	HCO_3^{-}	Mineralization degree
Content (mg/L)	103.75	165.15	21.52	1,948.25	1,388.09	1,689.25	1,823.79	7,139.80
Percentage (%)	5%	13.1%	0.55%	84.74%	37.6%	35.17%	29.89%	

pore size of 0.25 μm and porosity of 55% was selected for the experiment. Regarding the hollow fiber membrane module, its effective length, the number of fibers and effective membrane area are 90 cm, 2,250 and approximately 10 m^2, respectively.

2.1.3. Test scheme and instrument

As shown in Fig. 1, reverse osmosis concentrate brines on the feed side is pressed by a circulating pump into a membrane module for circulation. On the vacuum side, a vacuum pump is utilized for fresh water vapor pumping. Under the circumstance that the system runs steadily and normally, a Pt100 temperature sensor and a flow sensor are connected to an independently made intelligent acquisition system to measure temperature and flux at inlet and outlet of the membrane module where the feed solution flows. As for conductivities of feed solution inlet/outlet and fresh water on the vacuum side, they are tested by a conductivity meter. Additionally, temperature sensor, pressure sensor and a steam flow meter are adopted to measure temperature, pressure and flux of fresh water vapor on the vacuum side, respectively.

2.2. Mass transfer process of VMD

Transfer mechanism of MD is usually concluded as the following three steps: (i) feed solution is vaporized into water vapor on the feed side of membrane; (ii) water vapor migrates through non-invasive membrane; and (iii) the water vapor condenses on the permeate side of membrane. There exist two steps in transfer process of MD simultaneously, namely heat transfer and mass transfer. Driving force of heat transfer is determined by temperature difference between two sides of the membrane, while that of mass transfer depends on VPD incurred by vapor temperature difference on both sides of the membrane. It is obvious that mass and heat transfer processes are related to temperature difference on both sides of the membrane, which is theoretically confirmed as T_{mf}-T_{mp}. T_{mf} and T_{mp} are membrane surface temperatures on the thermal side and condensate side, respectively. As for the actual temperature difference, it is defined as the difference between feed temperature T_f on the feed side and vapor temperature T_p on the permeate side. Owing to the difference between temperature of main feed liquid on the feed side and that on membrane surface, temperature difference can be also found between membrane surface on the permeate side and fresh water vapor through the membrane, which is referred to temperature polarization. Coefficient of temperature polarization is defined as $\mathrm{TPC} = \frac{T_{mf} - T_{mp}}{T_f - T_p}$ [18]. Membrane surface temperature is unmeasurable in terms of the feed side and the permeate side, while temperature of the main feed liquid on feed side and fresh water vapor temperature on permeate side can be measured. It means that it is impossible for us to obtain theoretical temperature difference, but the actual temperature difference is attainable.

Mass transfer process of MD is divided into two processes: (i) a thermal side brine evaporation process on membrane surface, in which the vapor penetrates through membrane pore from the thermal side to the condensate side under the action of difference of partial pressure; (ii) vapor condensation on the permeate side. Therefore, partial pressure difference of vapor and permeability of membrane are two important factors in mass transfer process. And the mass flux of MD can be expressed as [19,20].

$$J = B_m \Delta P \tag{1}$$

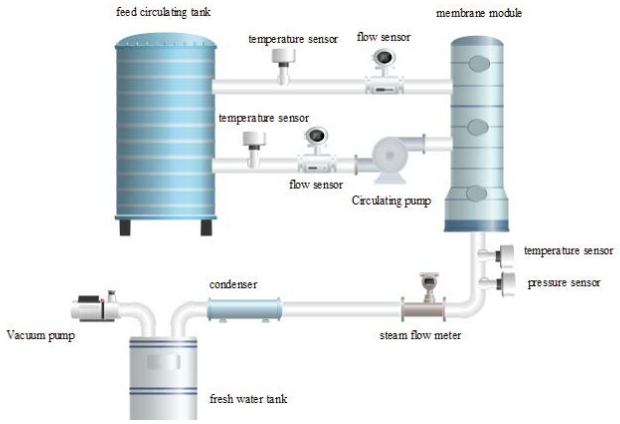

Fig. 1. Chart of a VMD system.

where B_m is the membrane distillation coefficient of MD, and ΔP is pressure difference.

2.2.1. Membrane distillation coefficient

The membrane distillation coefficient reflects permeability of the membrane and associated with permeability, porosity, average pore size and thickness of the membrane as well as pore tortuosity, etc. Therefore, different membrane structures generate different mass transfer processes. Mass transfer processes happening inside the membrane pore consist of Knudsen diffusion (K), Poiseuille diffusion (P) and molecular diffusion (M), or the combination of any two mechanisms among them.

As VMD is usually carried out under the total pressure between 10 and 50 kPa below vapor pressure of diffusate, there only exists air in trace amounts inside the membrane pore. Therefore, molecular diffusion resistance can be neglected because it is positively correlated to atmospheric partial pressure inside the membrane pore [4]. Hence, only Knudsen or Poiseuille model should be considered for VMD [19]. The type of mechanism occurring inside the membrane pore principally depends on mean free path l and pore diameter d_p of molecules inside the membrane pore. (i) If $l \ll d_p$ and $K_n = \frac{l}{d_p} < 0.01$, Poiseuille viscous flow forms and $B_m = \frac{1}{8\mu}\frac{\varepsilon r^2}{\tau\delta}\frac{MP_m}{RT_m}$ [21,22]; (ii) If $l \gg d_p$ and $K_n = \frac{l}{d_p} > 10$, Knudsen diffusion dominates and $B_m = \frac{2\varepsilon r}{3\tau\delta}\sqrt{\frac{8M}{\pi RT_m}}$ [20,21,22,23,24]; (iii) If $l \approx d_p$; Knudsen diffusion and Poiseuille viscous flow become comparative and $0.01 < K_n = \frac{l}{d_p} < 10$, $B_m = \frac{2\varepsilon r}{3\tau\delta}\sqrt{\frac{8M}{\pi RT_m}} + \frac{\varepsilon r^2 MP_m}{8\mu\tau\delta RT_m}$ [20,21,22,23] where ε stands for membrane porosity, r is pore radius, $\tau = \frac{(2-\varepsilon)^2}{\varepsilon}$ is pore tortuosity [20,25,26], δ is membrane thickness, M is the molecular weight of water, R is the gas constant, P_m is water vapor pressure inside the membrane pore in Pa, T_m is water vapor temperature inside the membrane pore, and μ is dynamic viscosity of water vapor inside the membrane pore.

Compared with pore diameter of membrane pore used for experiment, the mean free path of a molecule is adopted to determine mass transfer mechanism in VMD, which can be expressed as follows [21]:

$$l = \frac{K_B T_p}{P_p \sqrt{2}\pi\sigma^2} \tag{2}$$

Because only water vapor can pass through due to trace amounts of air in the membrane, parameters in the equation are all related to water vapor. In this equation, K_B is Boltzmann constant (1.381×10^{-23} J K^{-1}), σ is collision diameter of water vapor (2.641×10^{-10} m), and T_p and P_p represent the average temperature and the average pressure inside membrane pore, respectively.

It has been assumed that normal operating temperature of VMD ranges from 40°C to 80°C, corresponding to mean free path equivalent to l = 0.0201–0.0402 μm of molecules. As the average diameter of membrane pore is d_p = 0.25 μm, then l/d_p = 0.08–0.16. Therefore, mass transfer mechanism of VMD conforms to Knudsen diffusion and Poiseuille viscous flow, but closer to the latter.

2.2.2. Pressure difference

Pressure difference points to the difference between P_{mf} representing the vapor pressure on membrane surface of feed side and P_p denoting the total pressure on permeate side. For a VMD system, vapor on permeate side is associated with not only vapor pressure P_{mp} generated by vapor on membrane surface but also pressure P_v provided by vacuum pump. Therefore, VPD on both sides of VMD is written as follows:

$$\Delta P = \left(P_{\text{mf}} - P_{\text{mp}} - P_v\right) \tag{3}$$

Water vapor pressure is expressed by Antoine equation as follows [27]:

$$\ln P = A - \frac{B}{T + C} \tag{4}$$

where A, B and C are all constants, and T is water vapor temperature in °C. For water, A = 16.3872, B = 3,885.70 and C = 230.70 [27]. Hence, water vapor pressure can be expressed in

$$P = \exp\left(16.3872 - \frac{3885.70}{T + 230.70}\right) \tag{5}$$

Then

$$\Delta P = \left[\exp\left(16.3872 - \frac{3885.70}{T_{\text{mf}} + 230.70}\right) - \exp\left(16.3872 - \frac{3885.70}{T_{\text{mp}} + 230.70}\right) - P_v\right] \tag{6}$$

In this circumstance, water vapor flux passing through membrane pore is the osmotic flux

$$J = \left(\frac{2\varepsilon r}{3\tau\delta}\sqrt{\frac{8M}{\pi RT_{\text{mf}}}} + \frac{1}{8\mu}\frac{\varepsilon r^2}{\tau\delta}\frac{MP_{\text{mf}}}{RT_{\text{mf}}}\right)\left[\exp\left(16.3872 - \frac{3885.70}{T_{\text{mf}} + 230.70}\right) - \exp\left(16.3872 - \frac{3885.70}{T_{\text{mp}} + 230.70}\right) - P_v\right] \tag{7}$$

2.3. Experimental verification of mass transfer model

2.3.1. Model verification for water vapor pressure on vacuum side

In a measured VMD system, it is difficult to stabilize the pressure on the vacuum side. Analysis on the compositions

of the pressure on vacuum side demonstrates that it includes fresh water vapor pressure generated on the vacuum side and pressure provided by the vacuum pump. The former one can be figured out by Antoine equation, and the latter is equal to vacuum value of local atmospheric pressure (Yinchuan, Ningxia). Pressure on vacuum side can be expressed in

$$P_p = \exp\left(16.3872 - \frac{3885.70}{-46.13 + T_{mp}}\right) - P_v \quad (8)$$

where T_{mp} refers to vapor temperature in °C, and P_v is vacuum value of atmospheric pressure in Yinchuan that should be 893.3 HPa in winter and 881.4 HPa in summer (annual average: 887.35 HPa). Pressure on vacuum side can be calculated according to the formula and the results against vapor temperature are shown in Fig. 2. Meanwhile, pressure values on permeate side measured through experiment are also presented in the figure. Using R.Studio, the SSE is calculated to be 0.004 and the MAPE is 0.43. From the figure, we can find that the measured values in experiments are consistent with the calculated values by Eq. (8). Hence, computational formula of pressure on vacuum side is proven to be consistent with variation rules of such pressure of the experimental system. Additionally, Fig. 2 indicates that rise of vapor temperature leads to the reduction of pressure on the vacuum side.

2.3.2. Membrane flux model verification and modification

Eq. (7) was used to verify membrane flux of PTFE hollow fiber membrane applicable to this experiment. In the equation, ε was set at 55%, r at 0.25 μm, τ at 3.82, δ at 0.5 mm, M at 18 g/mol and R at 8.314 Pa m^3/(mol k). Additionally, P_{mf} is water vapor pressure inside membrane pore in Pa, and T_{mf} represents water vapor temperature inside it. As feed side circulates in the membrane module, both the temperatures of vapor entering the membrane and that passing out of the membrane can be measured. Temperature (unit: °C) inside membrane pore was calculated according to the mean value of inlet and outlet temperature values for membrane module on the feed side μ is dynamic viscosity (N/s m^2) of water vapor inside the membrane pore and calculated by μ = 0.0402 T_m + 8.022 (temperature range: 0°C–100°C). As shown in Fig. 3, theoretically calculated value of membrane flux substantially differs from its measured value in experiment under the combination of Knudsen diffusion and Poiseuille viscous flow. Using R.Studio, the SSE is calculated to be 120.74 and the MAPE is 89.17.

According to the experimental data, it has been found that the measured value of membrane flux is only related to Poiseuille viscous flow. This is consistent with the discussion about the relationship between mean free path l and pore diameter d_p in Section 1.1. The low Knudsen coefficient is mainly caused by Poiseuille viscous flow. However, the measured value of membrane flux is only 1/8 of the theoretical result. The reasons may lay on two aspects: (i) the experiment is conducted outside, which may be different from that in lab; (ii) present experiments handle numerous data compared with those in lab, hence the parameters associated with temperature and pressure is hard to control. With the large numbers of experimental data, we modified the membrane flux model that can be expressed as [8]:

$$J = \left(\frac{1}{64\mu}\frac{\varepsilon r^2}{\tau\delta}\frac{MP_{mf}}{RT_{mf}}\right)\left[\exp\left(16.3872 - \frac{3885.70}{T_{mf} + 230.70}\right) - \exp\left(16.3872 - \frac{3885.70}{T_{mp} + 230.70}\right) - P_v\right] \quad (9)$$

Based on the modification, we figure out the membrane flux by Eq. (9) and compare it with the measured flux in experiment in Fig. 4. Using R.Studio, the SSE is calculated to be 0.353 and the MAPE is 2.013. This confirms that the modified model can describe the membrane flux accurately.

3. Results and discussion

3.1. Simulation analysis on mass transfer mechanism analysis with membrane structure parameters

At present, most commonly used membrane materials of VMD include PTFE, PVDF and PP with different interior

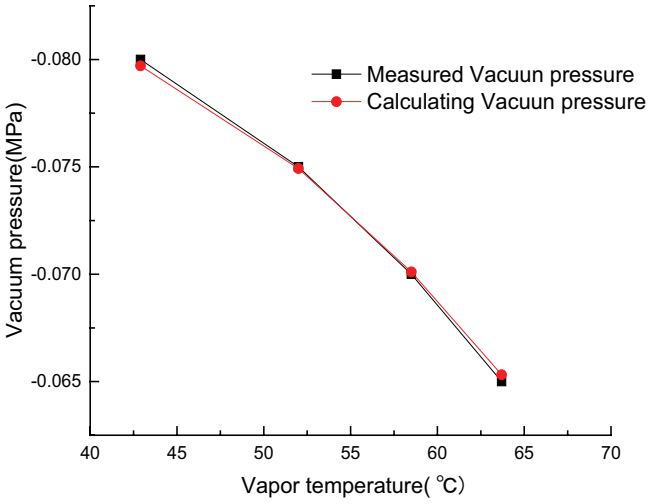

Fig. 2. Diagram of pressure curves on vacuum side.

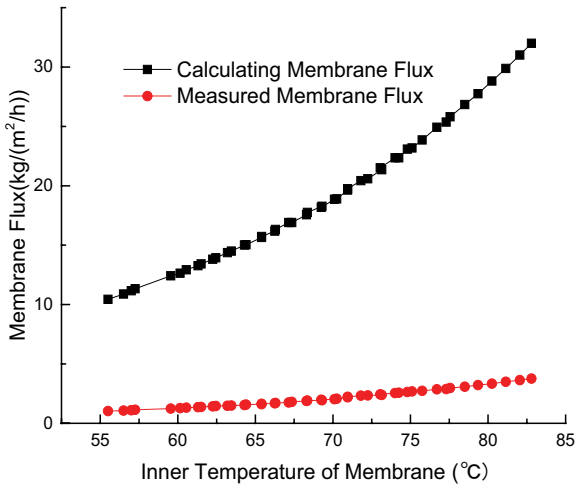

Fig. 3. Graph of theoretical membrane flux.

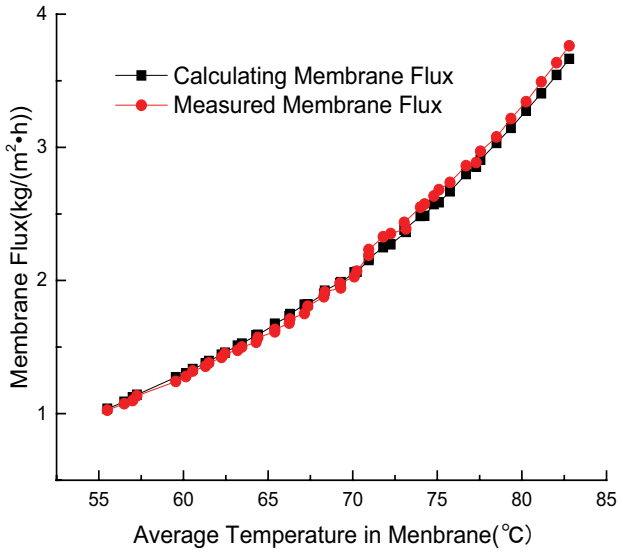

Fig. 4. Graph of modified membrane flux.

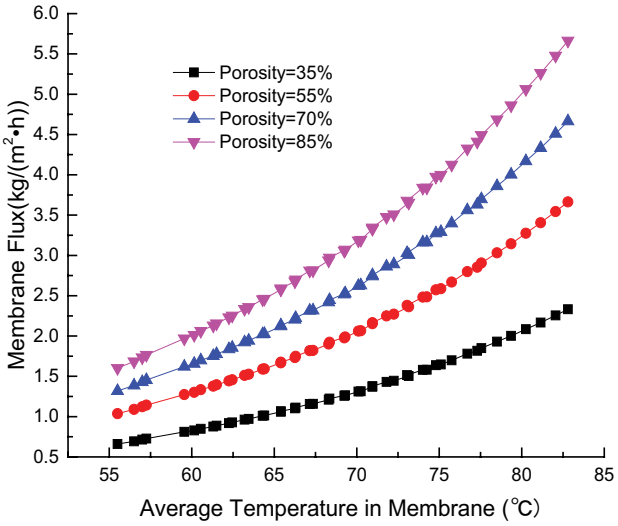

Fig. 5. Analysis diagram of the influence of porosity on membrane flux.

structures. Hence, their membrane flux values are also different from each other according to Eq. (9). In the following, this equation is adopted to analyze the influence of membrane structure on membrane flux. The membrane materials are presented in Table 2.

3.1.1. Influence of porosity on membrane flux

As shown in Table 2, several membrane materials with different values of porosity are selected to conduct analysis, namely, 35%, 55%, 70% and 85%. It can be observed from Fig. 5 that membrane flux with large porosity gradually increases with the temperature increase. For example, when temperature inside the membrane with porosity of 85% is 80°C, the membrane flux is 5 kg/(m²h). While it is 2 kg/(m²h) for the membrane with porosity of 35%. This presents that membrane materials with larger porosity should be selected to reach greatest membrane flux.

3.1.2. Influence of pore size on membrane flux

As shown in Table 2, a total of four typical pore sizes of the membrane are selected, including 0.1, 0.25, 0.45 and 0.6 μm, to analyze the membrane flux.

Eq. (9) indicates that membrane flux is proportional to square of membrane pore size. This is confirmed by the results shown in Fig. 6. For example, flux of the membrane with a pore size of 0.6 μm can be up to 18.86 kg/(m² h) when internal temperature is 80°C, while flux of membrane with 0.1 μm is only 0.52 kg/(m² h). Provided that only water vapor molecules can pass through the membrane, the greater the pore size is, the higher the membrane flux will be.

3.1.3. Influence of thickness on membrane flux

According to Table 2, we choose four typical thickness values, namely, δ = 50 μm, δ = 150 μm, δ = 290 μm and δ = 500 μm, to analyze its effect on the membrane flux.

Table 2
A list of common membrane materials for VMD

Membrane material	Membrane porosity (%)	Membrane thickness (μm)	Pore size of membrane (μm)	Tortuosity of membrane pore	Source
PTFE	70	175	0.25	2.41	[23]
PTFE	76.37	290	0.1052	3.8	[22]
	35.75	70	0.1303	6.3	
	81.47	50	0.1495	3.4	
PTFE	70	70	0.2	2.41	[18]
PTFE	90	64	0.2	1.34	
PTFE	89	77	0.45	1.38	
PVDF	62	126	0.22	3.07	
PVDF	66	116	0.45	2.72	
PVDF	85	150	0.16	1.56	[28]
PP	55	50	0.6	3.82	[29]

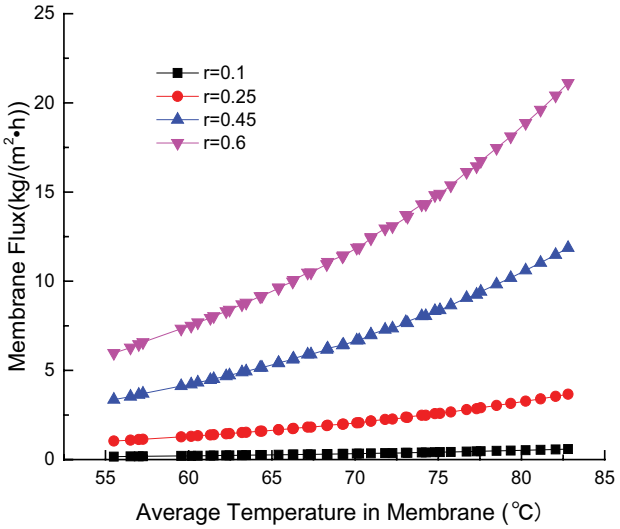

Fig. 6. Analysis diagram of the influence of pore size on membrane flux.

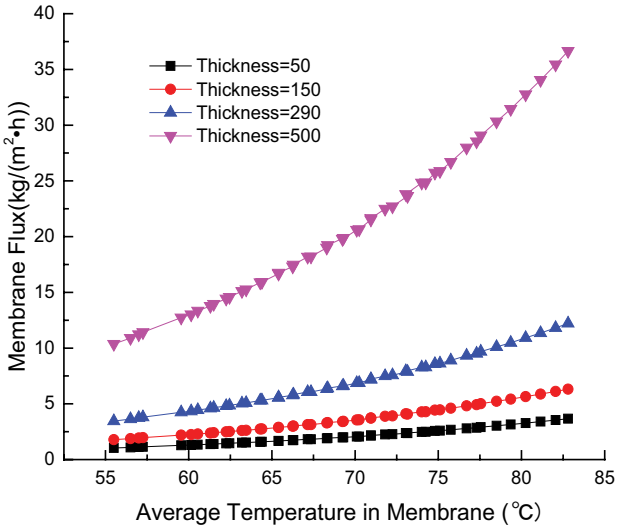

Fig. 7. Analysis diagram of the influence of thickness on membrane flux.

As shown in Fig. 7, when temperature inside the membrane is 80°C, the membrane flux with δ = 50 μm is 32.75 kg/(m² h). This is 10 times larger than that with δ = 500 μm. Therefore, the thinner the membrane is, the greater the membrane flux will be under the circumstance that mechanical strength has been satisfied. This may be explained that thicker membrane corresponds to longer path that the water vapor needs to pass, which results in greater resistance to the mass transfer process.

3.1.4. Influence of pore tortuosity

Pore tortuosity reflects degree of crook inside the membrane pore. Higher tortuosity means that the water vapor needs to go through a longer path of membrane pore and encounters greater resistance. According to $\tau = \frac{(2-\mu)^2}{\varepsilon}$, membrane porosity is inversely proportional to tortuosity. Therefore, membrane materials of a large porosity should be selected to obtain a small tortuosity. Based on Table 2, four typical tortuosity values were selected to analyze the membrane flux, namely, τ = 1.56, τ = 2.41, τ = 3.82 and τ = 6.3.

In Fig. 8, membrane flux, for example, with tortuosity 1.56 reaches 123.3 kg/(m² h), while that with tortuosity 6.3 is only 1.28 kg/(m² h), in the case that temperature inside the membrane is 80°C. Such a large difference proves that tortuosity has a significant influence on membrane flux.

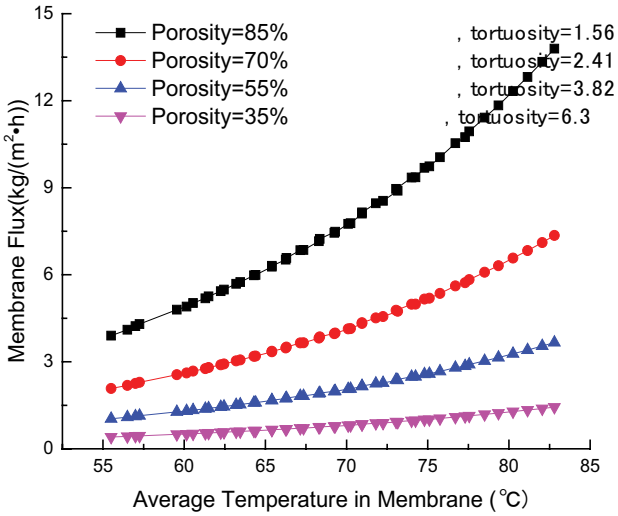

Fig. 8. Analysis diagram of the influence of pore tortuosity.

3.1.5. Membrane flux comparison among different membrane materials

Above analysis reveals that the larger the porosity and the pore size are, the greater the membrane flux will be. However, the higher the thickness and the tortuosity are, the lower the membrane flux will be. Under specific circumstances, these factors may compete each other. If values of porosity and pore size are higher, the membrane will be thinner. This will result in reduction of mechanical strength and service life of the membrane. During manufacturing and type selection for the membrane, membranes with larger porosity and pore size, but lower thickness values should be selected to reach greatest flux on the premise of ensuring strength and service life conditions for the membrane. To make a comparison, four types of membranes were selected according to Table 2, namely, #1 membrane (ε = 70%, *r* = 0.2 μm, δ = 70 μm, τ = 2.41), #2 membrane (ε = 85%, *r* = 0.16 μm, δ = 150 μm, τ = 1.56), #3 membrane (ε = 35.75%, *r* = 0.1495 μm, δ = 50 μm, τ = 6.3) and #4 membrane (ε = 55%, *r* = 0.25 μm, δ = 500 μm, τ = 3.82, used for the experiment). Relevant membrane flux values have been given in Fig. 9.

In the figure, #1 membrane is very thin and its membrane flux is the greatest although its porosity is not the highest. #2 membrane with the maximum porosity is rather thick and its membrane flux ranks second. Followed by #3 membrane with the minimum porosity, the smallest diameter, which

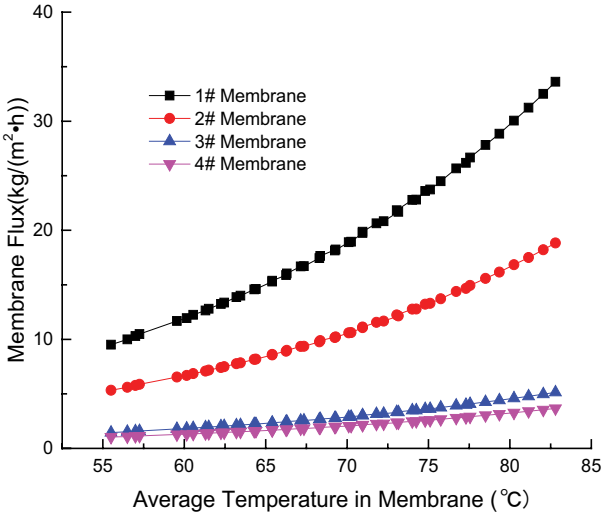

Fig. 9. Flux analysis diagram of membranes with different structures.

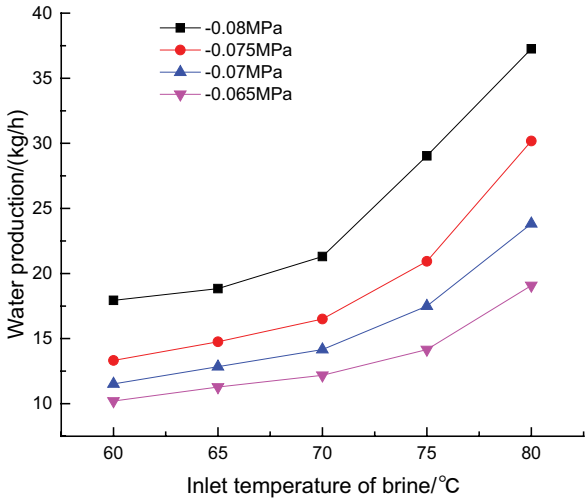

Fig. 10. Graph of different concentrate water inlet temperature values on fresh water yield.

is also the thinnest. Finally, the lowest flux occurs for the #4 membrane with intermediate porosity and diameter values, although it is the thickest. Through comparison, the maximum membrane flux is nearly six times greater than its minimum value. It illustrates that membrane structure has an enormous influence on membrane flux and all factors should be taken into consideration for the selection of membrane.

3.2. Experimental analysis on the influence of operating conditions on mass transfer mechanism

As mass transfer model of VMD only reflects impacts of membrane structure and VPD on both sides of the membrane on the membrane flux, it is an ideal model that only has the capability to reveal the influence of concentrate temperature and pressure on vacuum side on the flux. The operating conditions should also affect the membrane flux such as flow rate, concentration and membrane fouling, etc. The effects can be quantified by measured data in the experiments.

3.2.1. Influence of the inlet temperature of concentrate water on membrane flux

As shown in Fig. 10, when the room temperature is above 14°C, the degree of mineralization of concentrated water is 7.1 g/L, and the flux of the system is 4 m^3/h, for a specific vapor pressure (–0.065 MPa, –0.07 MPa, –0.075 MPa or –0.08 MPa), water yield of VMD increases with the increase of temperature. And in a specific temperature, for example, 80°C, and pressure –0.08 Mpa, water yield reaches maximum 37.62 kg/h. Additionally, the figure also indicates that if concentrate water inlet temperature is below 70°C, water yield goes up slowly as the temperature increases. While it dramatically increases after the temperature is higher than 70°C.

3.2.2. Influence of pressure on vacuum side on membrane flux

With the same environmental conditions (room temperature, degree of mineralization and flux of system),

Fig. 11 shows that when concentrate water inlet temperature is fixed, the water production increases with the rise of vacuum pressure on vapor side. And for a specific vacuum pressure, the water production increases with the increment of concentrate water inlet temperature. Owing to the limitation of the region choice where the experiments are conducted, vacuum pressure in Helan County is –0.083 MPa at the maximum. And it is impractical to keep vacuum pressure unchanged during operation process. The vacuum pressure may change with vapor temperature and vacuum pump running duration. Overall, the results demonstrate that the total water yield can be obtained based on instantaneous mass flow rate displayed on an orifice plate flow meter.

3.2.3. Influence of concentrate concentration on membrane flux

The operation runs 4 and a half hours under the conditions with vacuum pressure on vapor side –0.077 MPa and

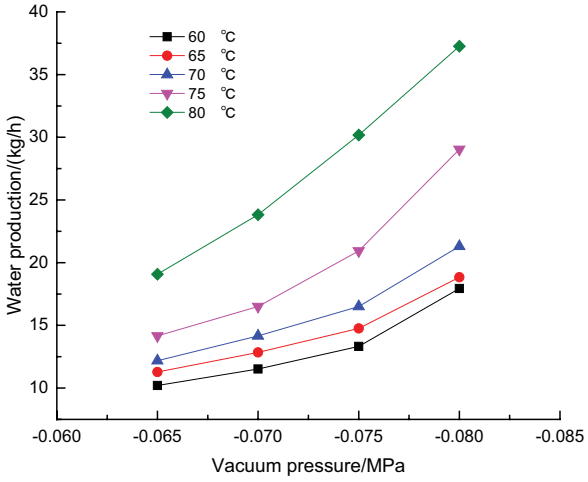

Fig. 11. Graph of the influence of different vacuum pressure values on fresh water yield.

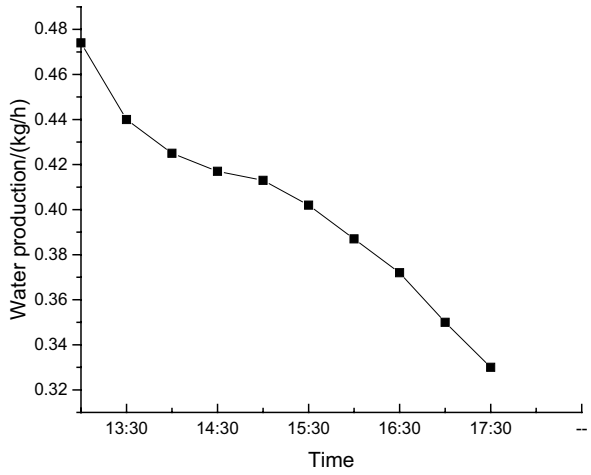

Fig. 12. Graph of the influence of different vacuum pressure values on fresh water yield.

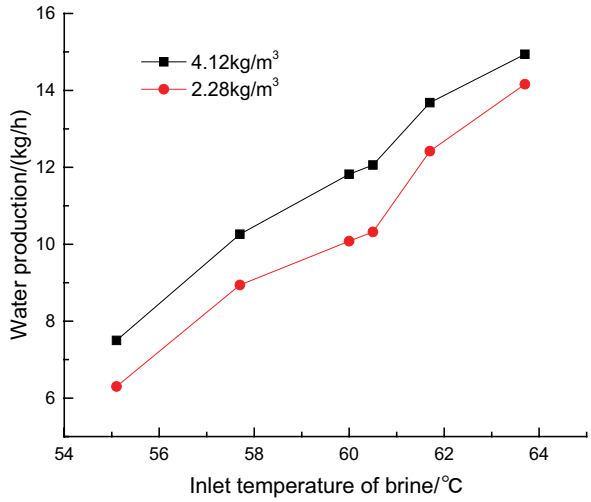

Fig. 13. Graph of the influence of different flow rates on fresh water yield.

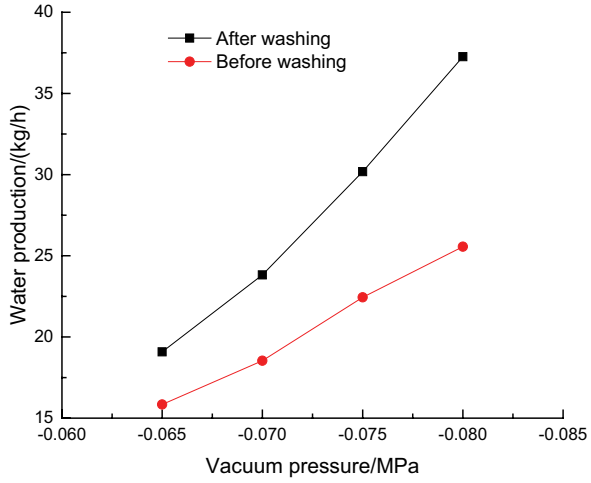

Fig. 14. Graph of the influence of membrane fouling on fresh water yield.

flow rate 1.85 kg/m^3. We find that the water yield decreases from 0.474 to 0.33 kg/m, while the conductivity increases from 6.73 to 11.82 μs/cm as shown in Fig. 12. This demonstrates that water yield decreases with the increment of concentrate concentration.

3.2.4. Influence of concentrate flow rate on membrane flux

We fix the pressure and choose two cases with flow rates 4.12 and 2.88 kg/m^3 to estimate the water yield of the VMD system. As shown in Fig. 13, water yield in the case of flow rate 4.12 kg/m^3 is higher than that in the case of flow rate 2.88 kg/m^3. It should be noted that water yield only has approximately 1 kg increase when the flow rate increases 1.5 times higher. It indicates that the flow rate has no significant influence on water yield.

3.2.5. Influence of membrane fouling on membrane flux

Since the VMD system has run for long time (1 year), the contaminants on membrane surface may accumulate and block brine circulating channel. The blockage may lead to the decrease of concentrate flow rate from about 4.2 kg/m^3 at the very beginning to roughly 2.5 kg/m^3. And it can also block the passing through of vapor, which may reduce the fresh water yield. As shown in Fig. 14, we compare the water yield against the vacuum pressure under the conditions before and after membrane cleaning. The concentrate water inlet temperature is set at 80°C. We find that the water yield under the case after membrane cleaning is significantly higher than that under the case before membrane cleaning. For example, when the vacuum pressure is –0.08 MPa, the increase of water yield can reach 11.7 kg/h after the membrane is cleaned.

4. Conclusions

- Heat and mass transfer model of VMD system is modified. For the mass transfer model, vacuum pressure on permeate side is corrected and verified by experimental data. Meanwhile, membrane flux model was also modified and verified. It has been deemed that mass transfer process of VMD is only related to Poiseuille viscous flow.
- The modified model is employed to conduct simulation analysis on the influence of various membrane structural parameters on membrane flux. The results manifest that larger porosity and pore diameter of the membrane pore lead to greater membrane flux. And thicker membrane with larger tortuosity results in lower membrane flux. Furthermore, membrane flux under different membrane materials is compared. It has been found that there exists no membrane possessing large porosity, large pore diameter, a low thickness value or small tortuosity at the same time. Consequently, all these parameters should be taken into account.
- Measured data are utilized to analyze the influence of operating conditions of the system on membrane flux. In addition, impacts of concentrate water inlet temperature, flow rate, concentration, pressure on the vacuum side and membrane fouling on membrane flux and fresh water yield are also analyzed. The results demonstrate

that temperature on the concentrate side and pressure on the vacuum side substantially affects membrane flux. However, flow rate and concentration of concentrate inflow have small influence on the membrane flux. The influence of membrane fouling is significant and the contaminants on the membrane surface should be regularly removed.

Symbols

T_{mf} — Temperatures at membrane surface on feed sides, °C
T_{mp} — Temperatures at membrane surface on permeate sides, °C
T_f — Feed temperature bulk temperatures of feed, °C
T_p — Feed temperature bulk temperatures of permeate, °C
B_m — Membrane distillation coefficient, kg m^{-2} s^{-1} Pa^{-1}
P_{mf} — Vapor pressure on membrane surface of feed side, Pa
P_{mp} — Vapor pressure on membrane surface of permeate side, Pa
P_p — Total pressure on permeate side, Pa
P_v — Vacuum pump pressure, Pa
l — Mean free path, nm
d_p — Mean pore size, μm
M — Molecular weight of water, kg mol^{-1}
R — Gas constant, J mol^{-1} K^{-1}
P_m — Water vapor pressure inside the membrane pore, Pa
T_m — Water vapor temperature inside the membrane pore, °C
K_B — Boltzmann's constant, J K^{-1}

Greek

ε — Membrane porosity, %
r — Membrane pore radius, μm
τ — Membrane pore tortuosity
δ — Membrane thickness, μm
μ — Water dynamic viscosity, kg m^{-1} s^{-1}
σ — Collision diameter of water vapour, m

Subscripts

mf — Hydrophobic surface of the membrane at the feed side
mp — Hydrophobic surface of the membrane at the permeate side
f — Feed
p — Permeate
v — Vapour phase
M — Membrane

Acknowledgments

This study was supported by National Natural Scientific Foundation of China (No. 51469027) and Public welfare industry (agriculture) research special fund project (201203003-4) and 1st Class Discipline Construction Project of Institutions of Higher Learning in Ningxia (NXYLXK2017A03);

References

[1] M. Safavi, T. Mohammadi, High-salinity water desalination using VMD, Chem. Eng. J., 149 (2009) 191–195.
[2] M.S. El-Bourawi, Z. Ding, R. Ma, M. Khayet, A framework for better understanding membrane distillation separation process, J. Membr. Sci., 285 (2006) 4–29.
[3] B. Li, K.K. Sirkar, Novel membrane and device for direct contact membrane distillation-based desalination process, J. Membr. Sci., 257 (2005) 60–75.
[4] J.I. Mengual, M. Khayet, M.P. Godino, Heat and mass transfer in vacuum membrane distillation, Int. J. Heat Mass Transfer, 47 (2004) 865–875.
[5] S.B. Abdallah, N. Frikha, S. Gabsi, Simulation of solar vacuum membrane distillation unit, Desalination, 324 (2013) 87–92.
[6] J.G. Lee, W.S. Kim, Numerical modeling of the vacuum membrane distillation process, Desalination, 331 (2013) 46–55.
[7] A.S. Kim, H.S. Lee, D.S. Moon, H.J. Kim, Statistical theory of vapor transport through hollow fiber membranes in vacuum membrane distillation: effusion analogy, Desalination, 410 (2017) 77–90.
[8] J. Liu, M. Liu, H. Guo, W. Zhang, K. Xu, B. Li, Mass transfer in hollow fiber vacuum membrane distillation process based on membrane structure, J. Membr. Sci., 532 (2017) 115–123.
[9] G.J. Florez, C. Salvatore, V. Anton, S. Clara, Multi-scale hybrid numerical model for the study of mass transfer through a microporous artificial membrane, Heat Mass Transfer, 2018.
[10] M. Taherinejad, J. Gorman, E. Sparrow, S. Derakhshan, Porous medium model of a hollow-fiber water filtration system, J. Membr. Sci., 563 (2018) 210–220.
[11] B. Martijn, B. Niels, N. Bart, Modeling of semibatch air gap membrane distillation, Desalination, 430 (2018) 98–106.
[12] Q.M. Ma, A. Aras, C. Corinne, Direct integration of a vacuum membrane distillation module within a solar collector for small-scale units adapted to seawater desalination in remote places: Design, modeling & evaluation of a flat-plate equipment, J. Membr. Sci., 564 (2018) 617–633.
[13] J.C. Wang, X.C. Gao, G.Z. Ji, X.H. Gu, CFD simulation of hollow fiber supported NaA zeolite membrane modules, Sep. Purif. Technol., 213 (2019) 1–10.
[14] S. Abdolbaghi, H.R. Mahdavi, T. Mohammadi, Simulation of heat and mass transport for ethylene glycol solution separation using a vacuum membrane distillation process, Desal. Wat. Treat., 148 (2019) 30–41.
[15] C.Y. Ma, Y.B. Liu, F. Li, C.S. Shen, M.H. Huang, Z.W. Wang, C. Cao, Q.Z. Zhou, Y.Z. Sheng, W. Sand, CFD simulations of fiber-fiber interaction in a hollow fiber membrane bundle: fiber distance and position matters, Sep. Purif. Technol., 209 (2019) 707–713.
[16] B. Yang, H. Chen, C. Ye, X. Li, Y. Feng, Experimental and numerical simulation to investigate the effects of membrane fouling on the heat and mass transfer, Int. J. Thermophys., 40 (2019) 8.
[17] P. Yazgan-Birgi, M.I. Hassan Ali, H.A. Arafat, Comparative performance assessment of flat sheet and hollow fiber DCMD processes using CFD modeling, Sep. Purif. Technol., 212 (2019) 709–722.
[18] J. Phattaranawik, R. Jiraratananon, A.G. Fane, Heat transport and membrane distillation coefficients in direct contact membrane distillation, J. Membr. Sci., 212 (2003) 177–193.
[19] K.W. Lawson, D.R. Lloyd, Membrane distillation. I. Module design and performance evaluation using vacuum membrane distillation, J. Membr. Sci., 120 (1996) 111–121.
[20] J.C. Cai, F. Guo, Study of mass transfer coefficient in membrane desalination, Desalination, 407 (2017) 46–51.
[21] A. Cipollina, M.G.D. Sparti, A. Tamburini, G. Micale, Development of a membrane distillation module for solar energy seawater desalination, Chem. Eng. Res. Design, 90 (2012) 2101–2121.
[22] H. Zhang, M. Liu, D. Sun, B. Li, P. Li, Evaluation of commercial PTFE membranes for desalination of brine water through vacuum membrane distillation, Chem. Eng. Process. Process Intensif., 110 (2016) 52–63.

[23] M. Qtaishat, T. Matsuura, B. Kruczek, M. Khayet, Heat and mass transfer analysis in direct contact membrane distillation, Desalination, 219 (2008) 272–292.
[24] K. Smolders, A.C.M. Franken, Terminology for membrane distillation, Desalination, 72 (2017) 249–262.
[25] S.B. Iversen, V.K. Bhatia, K. Damjohansen, G. Jonsson, Characterization of microporous membranes for use in membrane contactors, J. Membr. Sci., 130 (1997) 205–217.
[26] S. Srisurichan, R. Jiraratananon, A.G. Fane, Mass transfer mechanisms and transport resistances in direct contact membrane distillation process, J. Membr. Sci., 277 (2006) 186–194.
[27] J.M. Smith, H.C. Van Ness, M.M. Abbott, Introduction to Chemical Engineering Thermodynamics, 7/e, 1975.
[28] D. Liu, C. Wu, X.L. Lv, Study on vacuum membrane distillation process for the desalination-concentration of a reverse osmosis drained wastewater from a petrochemical plant, Technol. Water Treat., 35 (2009) 60–63.
[29] L. Li, Q. Kuang, L. Min, J. Zhang, Study of brackish water desalination by vacuum membrane distillation. Technol. Water Treat., 33 (2007) 67–70.